Volume 104 Number 2 March 2007 ISSN 0022-4073
website: http://www.elsevier.com/locate/jqsrt

Journal of Quantitative Spectroscopy & Radiative Transfer

SPECIAL ISSUE

EUROTHERM SEMINAR 78—COMPUTATIONAL THERMAL RADIATION IN PARTICIPATING MEDIA II

Guest Editors:
D. Lemonnier, N. Selçuk, P. Lybaert and M.P. Mengüç

ELSEVIER

Journal of Quantitative Spectroscopy & Radiative Transfer 104 (2007) 217–227

Journal of Quantitative Spectroscopy & Radiative Transfer

www.elsevier.com/locate/jqsrt

Elliptic PDE formulation of general, three-dimensional high-order P_N-approximations for radiative transfer

Jun Yang, Michael F. Modest*

Department of Mechanical and Nuclear Engineering, The Pennsylvania State University, University Park, PA 16802, USA

Received 10 July 2006; accepted 28 July 2006

Abstract

A new methodology is presented for the application of the spherical harmonics method (P_N) to decompose the radiative transfer equation (RTE) into a set of coupled second-order partial differential equations, allowing for variable properties and arbitrary three-dimensional geometries. The proposed methodology employs successive elimination of spherical harmonic tensors, thus reducing the number of first-order partial differential equations needed to be solved simultaneously by previous P_N-approximations ($=(N+1)^2$). The result is a relatively small set ($=N(N+1)/2$) of second-order, elliptic partial differential equations, which can be solved with standard PDE solution packages. Moreover, the general boundary conditions and supplementary conditions to be used in the P_N-approximation are formulated for arbitrary three-dimensional geometries. Numerical computations are carried out with the P_3-approximation for several one-dimensional and two-dimensional problems with emitting, absorbing and scattering media, using both constant and variable properties. Results are compared to analytical solutions and discrete ordinates simulations and a discussion of ray effects and false scattering is provided.

1. Introduction

Exact analytical solutions to the equation of radiative transfer are exceedingly difficult to obtain and explicit solutions are only possible for very simple situations, such as one-dimensional plane-parallel media without scattering. For more complicated scenarios, which may involve radiative equilibrium, multi-dimensional irregular geometry, anisotropic scattering or inhomogeneous media, several approximate methods have been developed over time. Among these approximate methods, the *spherical harmonics method* (SHM) or a variation of it, the *discrete ordinates method* (DOM) or the *finite volume method* (FVM), the *zonal method* and the *Monte Carlo method* have been used most frequently for the majority of radiative heat transfer analysis [1]. Unlike the *zonal method*, both the SHM and DOM/FVM approximate the directional variation of the radiative intensity rather than its spatial behavior. However, the underlying approaches to represent the directional dependence of radiative intensity for SHM and DOM/FVM are quite different. The DOM employs a discrete representation of the directional variation with integrals over total solid angle 4π obtained via

*Corresponding author. Fax: +1 814 863 8682.
E-mail address: mfm6@psu.edu (M.F. Modest).

0022-4073/$ - see front matter © 2006 Elsevier Ltd. All rights reserved.
doi:10.1016/j.jqsrt.2006.07.017

Nomenclature

A_i	phase function coefficients
$D^n_{mm'}$	Wigner function
I	radiative intensity
I^m_n	intensity coefficient function
J	spherical harmonics series
$\mathscr{L}$	differential operator
L	slab thickness
P^m_n	associated Legendre polynomial
R	direction vector length
$\hat{s}, \vec{s}$	(unit) direction vector
Y^m_n	spherical harmonic

Greek symbols

α, γ	property parameters
β	extinction coefficient
δ	surface rotation angle
κ	absorption coefficient
θ	polar angle
μ	$\equiv \cos\theta$
σ_s	scattering coefficient
τ	optical coordinate
Φ	scattering phase function
ω	single scattering albedo
Ω	solid angle

Subscripts

b	blackbody
w	wall

numerical quadrature, while the SHM captures the directional distribution of intensity by expressing it into a series of spherical harmonics. The DOM/FVM method is relatively simple to implement, but has several drawbacks, such as the fact that an iterative solution is required in the presence of scattering media or reflecting walls. In addition, its convergence is known to slow down for optically thick media. Furthermore, DOM may suffer ray effects and possibly false scattering due to its angular discretization [2]. Statistical methods like the *Monte Carlo method* can solve the most complicated problems with relative ease, but they are always subject to statistical error and require great computational power. The SHM has several advantages over other approximation methods: first, it converts the integro-differential radiative transfer equation (RTE) into relatively simple partial differential equations, which can be solved by using standard PDE solver packages. In this study, a set of coupled second-order PDEs is derived for an arbitrary order P_N approximation. Second, since the SHM is a spectral method, it should require fewer terms than DOM for similar accuracy. Unlike DOM/FVM, CPU time requirements for SHM do not increase for scattering media and reflecting walls.

The lowest-order P_N-approximation, the P_1-approximation, has enjoyed great popularity because of its relative simplicity and compatibility with standard methods for the solution of the energy equation [1]. However, the P_1-approximation performs poorly in the optically thin limit and other nonisotropic radiative intensity fields. On the downside, mathematical complexity increases rapidly if higher-order

P_N-approximations for multi-dimensional geometry are desired, which is probably responsible for the fact that its development lags behind that for the DOM/FVM.

A number of higher-order P_N-approximations have been formulated for specific geometries by exploiting the symmetry of the media confined in either one-dimensional slabs, concentric cylinders or concentric spheres. Kofink [3] gave a general P_N-approximation for one-dimensional cylindrical media when solving the Boltzmann equation for neutron transport. Bayazitoğlu and Higenyi [4] limited their development to the P_3 calculation of one-dimensional cylindrical and spherical media. Tong and Swathi [5] obtained higher-order solutions up to P_{11} for an anisotropically scattering medium between one-dimensional concentric spheres. Ratzel and Howell [6] studied a gray absorbing and emitting medium in a two-dimensional rectangular enclosure using the moments of intensity based on the P_3 differential approximation. Similarly, Mengüç and Viskanta [7] also numerically investigated the P_1- and P_3-approximations in a three-dimensional rectangular enclosure by employing the moments of intensity. For general geometries with isotropic scattering, Davison [8] has formulated a P_N-transformation of the Boltzmann equation into $(N+1)^2$ PDEs for constant property media. Finally, Ou and Liou [9] derived the three-dimensional P_N-approximation for arbitrary coordinate systems resulting in a set of $(N+1)^2$ complex, coupled, first-order PDEs similar to DOM, without, however, discussing boundary conditions. Here we present a new generic methodology that decomposes the RTE into $N(N+1)/2$ coupled second-order elliptic partial differential equations for a given odd order N, allowing for variable properties and arbitrary three-dimensional geometries. The formulation is accompanied by a set of generic boundary conditions.

The methodology is outlined in detail for the P_3-approximation, and tested extensively with several one- and two-dimensional problems, with constant as well as variable properties, by comparison with analytical as well as DOM/FVM results.

2. Mathematical formulation

For a given location $\vec{\tau}$ under optical coordinates based on the extinction coefficient β, i.e., $\mathrm{d}\vec{\tau} = \beta\,\mathrm{d}s$, where s is path length, let $\vec{s}$ be a vector of arbitrary magnitude R, such that $\vec{s} = R\hat{s}$, with $\hat{s}$ being a unit direction vector. Following Davison [8], we may express the intensity field $I(\vec{\tau},\hat{s})$ in terms of an infinite series

$$I(\vec{\tau},\hat{s}) = \frac{1}{4\pi}\sum_n [(2n+1)J_n(\vec{\tau},\vec{s})]_{R=1}, \tag{1}$$

where

$$J_n = \frac{1}{2n+1}\sum_{m=-n}^{n} I_n^m(\vec{\tau})\,Y_n^m(\vec{s}). \tag{2}$$

In Eq. (2) the $I_n^m(\vec{\tau})$ are location-dependent coefficient functions associated with a given spherical harmonic $Y_n^m(\vec{s})$, while directional-dependency of the intensity field is resolved in terms of a series of integral-degree real spherical harmonics defined as [10]

$$Y_n^m(R,\theta,\phi) = \begin{cases} R^n\cos(m\phi)P_n^m(\cos\theta) & \text{for } m \geqslant 0, \\ R^n\sin(m\phi)P_n^m(\cos\theta) & \text{for } m < 0, \end{cases} \tag{3}$$

and $P_n^m(\cos\theta)$ are *associated Legendre polynomials*.

The general equation of radiative transfer has the form [1]

$$\hat{s}\cdot\nabla_\tau I + I = (1-\omega)I_\mathrm{b} + \frac{\omega}{4\pi}\int_{4\pi} I(\hat{s}')\Phi(\hat{s}\cdot\hat{s}')\,\mathrm{d}\Omega', \tag{4}$$

where ω is the single scattering albedo, Φ is the scattering phase function and Ω is solid angle. The intensity gradient, ∇_τ, along direction $\hat{s}$ is written in terms of nondimensional optical coordinates. Substituting Eq. (1)

into the RTE, we find

$$\left[\sum_{n=0}^{N}(2n+1)\hat{s}\cdot\nabla_\tau J_n\right]_{R=1} = -\left[\sum_{n=0}^{N}(2n+1)J_n\right]_{R=1} + (1-\omega)4\pi I_b + \frac{\omega}{4\pi}\int_{4\pi}\left[\sum_{n=0}^{N}(2n+1)J_n(\vec{\tau},\hat{s}')\right]_{R=1}\Phi(\hat{s}\cdot\hat{s}')\,d\Omega'. \tag{5}$$

For *anisotropic scattering* the scattering phase function Φ is expanded into *Legendre polynomials* [1]. Collecting spherical harmonics of order n, one obtains

$$\nabla_s\cdot\nabla_\tau J_{n+1} + \alpha_n J_n + \left[(2n-1)\hat{s} - R^2\nabla_s\right]\cdot\nabla_\tau J_{n-1} = 4\pi(1-\omega)I_b\delta_{n0} \tag{6}$$

where

$$\alpha_n = (2n+1) - \omega A_n, \tag{7}$$

and δ_{n0} is Kronecker's delta.

Since we have collected the nth order harmonics, Eq. (6) constitutes a set of $2n+1$ independent PDEs of first order in space. However, to construct elliptic second order PDEs and, thus, to reduce the number of PDEs, every odd order J_n may be eliminated, leading to

$$-\nabla_\tau\left(\frac{1}{\alpha_{n+1}}\nabla_\tau\right)^T : \nabla_s\nabla_s J_{n+2} - \nabla_\tau\left(\frac{1}{\alpha_{n-1}}\nabla_\tau\right)^T : \mathscr{L}_{n-1}\mathscr{L}_{n-2}J_{n-2} - \left[\nabla_\tau\left(\frac{1}{\alpha_{n+1}}\nabla_\tau\right)^T : \nabla_s\mathscr{L}_n - \alpha_n + \nabla_\tau\left(\frac{1}{\alpha_{n-1}}\nabla_\tau\right)^T : \mathscr{L}_{n-1}\nabla_s\right]J_n = 4\pi(1-\omega)I_b\delta_{n0}, \tag{8}$$

where $\mathscr{L}_{n-1} = [(2n-1)\hat{s} - R^2\nabla_s]$ is an operator and $\nabla_s\nabla_s$, $\nabla_s\mathscr{L}$, $\mathscr{L}\nabla_s$ and $\mathscr{L}\mathscr{L}$ are simply different combinations of the two basic operators ∇_s and $\mathscr{L}$. After rather tedious algebra, the three components of the operator ∇_s on a given spherical harmonic Y_n^m is obtained as

$$\begin{aligned}\frac{Y_n^m}{\partial s_x} &= -\frac{1}{2}(n+m)(n+m-1)Y_{n-1}^{m-1} + \frac{1}{2}Y_{n-1}^{m+1}, \quad m\geqslant 1,\\ &= Y_{n-1}^1, \quad m=0,\\ &= -\frac{1}{2}(n-m)(n-m-1)Y_{n-1}^{m+1}(1-\delta_{m,-1}) + \frac{1}{2}Y_{n-1}^{m-1}, \quad m\leqslant -1,\end{aligned} \tag{9a}$$

$$\begin{aligned}\frac{\partial Y_n^m}{\partial s_y} &= \frac{1}{2}(n+m)(n+m-1)Y_{n-1}^{1-m}(1-\delta_{m,1}) + \frac{1}{2}Y_{n-1}^{-m-1}, \quad m\geqslant 1,\\ &= Y_{n-1}^{-1}, \quad m=0,\\ &= -\frac{1}{2}(n-m)(n-m-1)Y_{n-1}^{-m-1} - \frac{1}{2}Y_{n-1}^{1-m}, \quad m\leqslant -1,\end{aligned} \tag{9b}$$

$$\frac{\partial Y_n^m}{\partial s_z} = (n+|m|)Y_{n-1}^m \quad \text{all } m. \tag{9c}$$

Similarly, $\mathscr{L}_n Y_n^m$ can be shown to be

$$\begin{aligned}\mathscr{L}_{n,x}Y_n^m &= -\frac{1}{2}[Y_{n+1}^{m+1} - (n-m+2)(n-m+1)Y_{n+1}^{m-1}], \quad m\geqslant 1,\\ &= -Y_{n+1}^1, \quad m=0,\\ &= -\frac{1}{2}[Y_{n+1}^{m-1} - (n+m+2)(n+m+1)Y_{n+1}^{m+1}(1-\delta_{m,-1})], \quad m\leqslant -1,\end{aligned} \tag{10a}$$

$$\begin{aligned}\mathscr{L}_{n,y}Y_n^m &= -\tfrac{1}{2}[Y_{n+1}^{-m-1} + (n-m+2)(n-m+1)Y_{n+1}^{1-m}(1-\delta_{m,1})], \quad m \geqslant 1,\\ &= -Y_{n+1}^{-1}, \quad m = 0,\\ &= \frac{1}{2}[Y_{n+1}^{-m+1} + (n-m+2)(n-m+1)Y_{n+1}^{-m-1}], \quad m \leqslant -1,\end{aligned} \tag{10b}$$

$$\mathscr{L}_{n,z}Y_n^m = (n-|m|+1)Y_{n+1}^m \quad \text{all } m. \tag{10c}$$

Substituting these relations into Eq. (8), it is found that, for an even order n, there are exactly $(2n+1)$ independent spherical harmonics. Therefore, $(2n+1)$ independent PDEs can be constructed by collecting spatial derivatives of the I_n^m, corresponding to each independent spherical harmonic. For the P_N-approximation, there are total of $N(N+1)/2$ PDEs that can be obtained from this method, as shown in the next section for a sample set of PDEs from the P_3-approximation.

Following the discussion in the previous section and letting $N=3$, we will extract the P_3-approximation. Applying Eq. (8) for $n=0$ and $n=2$, and using $J_4=0$ for the P_3-approximation and $\nabla_s J_0 = 0$ since $Y_0 \equiv 1$, the equations contain a total of six independent spherical harmonics (Y_2^m and Y_0). By collecting coefficients of each spherical harmonic via the tools presented in the previous section, six PDEs can be obtained for a three-dimensional problem. Here we will limit our study to a two-dimensional enclosure without dependence in the z-direction (as shown in Fig. 1). Due to the symmetry of the intensity field about the x–y-plane, which requires $I(\theta,\phi) = I(\pi-\theta,\phi)$, the coefficients associated with spherical harmonics Y_2^{-1} and Y_2^1 are then shown to be zero (as well as I_1^0, I_3^{-2}, I_3^0 and I_3^2, i.e., all with $n+m$ odd). Thus, the six PDEs from Eq. (8) reduce to four coupled elliptic PDEs as summarized below

$$\begin{aligned}&\frac{\partial}{\partial\tau_x}\left[2\gamma_{8,3}\frac{\partial I_2^{-2}}{\partial\tau_x} - \gamma_{1,1}\frac{\partial I_2^0}{\partial\tau_y} + 2\gamma_{7,-3}\frac{\partial I_2^2}{\partial\tau_y} + \frac{5}{\alpha_1}\frac{\partial I_0}{\partial\tau_y}\right]\\ &+\frac{\partial}{\partial\tau_y}\left[2\gamma_{8,3}\frac{\partial I_2^{-2}}{\partial\tau_y} - \gamma_{1,1}\frac{\partial I_2^0}{\partial\tau_x} - 2\gamma_{7,-3}\frac{\partial I_2^2}{\partial\tau_x} + \frac{5}{\alpha_1}\frac{\partial I_0}{\partial\tau_x}\right] - 2\alpha_2 I_2^{-2} = 0 \quad \text{for } Y_2^{-2},\end{aligned} \tag{11a}$$

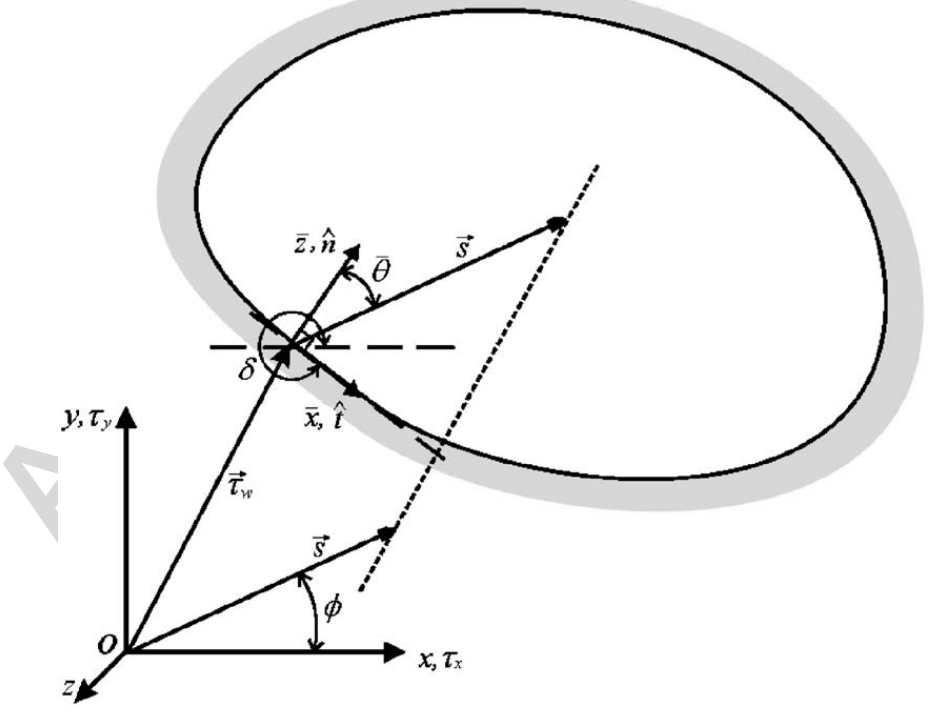

Fig. 1. Local and global coordinates for a two-dimensional enclosure.

$$\frac{\partial}{\partial\tau_x}\left[\gamma_{6,1}\frac{\partial I_2^0}{\partial\tau_x}-6\gamma_{1,1}\frac{\partial I_2^2}{\partial\tau_x}-6\gamma_{1,1}\frac{\partial I_2^{-2}}{\partial\tau_y}-\frac{5}{\alpha_1}\frac{\partial I_0}{\partial\tau_x}\right]$$
$$+\frac{\partial}{\partial\tau_y}\left[\gamma_{6,1}\frac{\partial I_2^0}{\partial\tau_y}+6\gamma_{1,1}\frac{\partial I_2^2}{\partial\tau_y}-6\gamma_{1,1}\frac{\partial I_2^{-2}}{\partial\tau_x}-\frac{5}{\alpha_1}\frac{\partial I_0}{\partial\tau_y}\right]-\alpha_2 I_2^0=0 \quad \text{for } Y_2^0, \tag{11b}$$

$$\frac{\partial}{\partial\tau_x}\left[2\gamma_{8,3}\frac{\partial I_2^2}{\partial\tau_x}-\gamma_{1,1}\frac{\partial I_2^0}{\partial\tau_x}-2\gamma_{7,-3}\frac{\partial I_2^{-2}}{\partial\tau_y}+\frac{5}{\alpha_1}\frac{\partial I_0}{\partial\tau_x}\right]$$
$$+\frac{\partial}{\partial\tau_y}\left[2\gamma_{8,3}\frac{\partial I_2^2}{\partial\tau_y}+\gamma_{1,1}\frac{\partial I_2^0}{\partial\tau_y}+2\gamma_{7,-3}\frac{\partial I_2^{-2}}{\partial\tau_x}-\frac{5}{\alpha_1}\frac{\partial I_0}{\partial\tau_y}\right]-2\alpha_2 I_2^2=0 \quad \text{for } Y_2^2, \tag{11c}$$

$$\frac{\partial}{\partial\tau_x}\left[\frac{5}{\alpha_1}\frac{\partial I_0}{\partial\tau_x}-\frac{1}{\alpha_1}\frac{\partial I_2^0}{\partial\tau_x}+\frac{6}{\alpha_1}\frac{\partial I_2^2}{\partial\tau_x}+\frac{6}{\alpha_1}\frac{\partial I_2^{-2}}{\partial\tau_y}\right]$$
$$+\frac{\partial}{\partial\tau_y}\left[\frac{5}{\alpha_1}\frac{\partial I_0}{\partial\tau_y}-\frac{1}{\alpha_1}\frac{\partial I_2^0}{\partial\tau_y}-\frac{6}{\alpha_1}\frac{\partial I_2^2}{\partial\tau_y}+\frac{6}{\alpha_1}\frac{\partial I_2^{-2}}{\partial\tau_x}\right]=5\alpha_0(I_0-4\pi I_b) \quad \text{for } Y_0, \tag{11d}$$

where

$$\gamma_{i,j}=\left(\frac{i}{\alpha_3}+\frac{j}{\alpha_1}\right).$$

Since intensity is expressed as a truncated series of spherical harmonics, Eqs. (1)–(3), boundary conditions can only be satisfied approximately. This is done by minimizing the difference between $I(\vec{\tau}=\vec{\tau}_w,\hat{s})$ and $I_w(\vec{\tau}_w,\hat{s})$ over the hemisphere covering all outgoing directions $\hat{n}\cdot\hat{s}>0$ everywhere on the surface, as described by vector $\vec{\tau}_w$ and shown in Fig. 1. There are several minimization schemes, the most popular ones proposed by Mark [11,12] and by Marshak [13]. For more general problems, Marshak's boundary condition appears to be more flexible and accurate since it minimizes the difference in an integral sense. Here, Marshak's boundary conditions are used, i.e.,

$$\int_{\hat{n}\cdot\hat{s}>0} I(\vec{\tau}_w,\vec{s})\,\bar{Y}_{2i-1}^m\,d\Omega=\int_{\hat{n}\cdot\hat{s}>0} I_w(\vec{s})\,\bar{Y}_{2i-1}^m\,d\Omega,\quad i=1,2,\ldots,\tfrac{1}{2}(N+1)\ \text{ all relevant } m, \tag{12}$$

where the $\bar{Y}$ denote spherical harmonics measured from a local spherical coordinate system, with polar angle $\bar{\theta}$ measured from the surface normal (local $\bar{z}$-axis), and $\bar{\phi}$ in the plane of the surface (measured from a local $\bar{x}$-axis). "All relevant m" implies choosing a set consistent with the P_N-approximation. For example, for the P_3-approximation six boundary conditions are needed: $i=1$ provides three ($m=-1,0,+1$), and another three must come from $i=2$ (usually chosen as the smallest m-values, i.e., $m=-1,0,+1$).

In general, of course, the local surface normal does not coincide with the global z-axis. Thus, in order to obtain a generic boundary condition for arbitrary geometries the global spherical harmonics must be rotated into the local coordinate system for the evaluation of Eq. (12). This can be done by expressing intensity in terms of, both, local and global coordinates:

$$I(\vec{\tau},\vec{s})=\frac{1}{4\pi}\sum_n^N\sum_{m=-n}^n I_n^m(\vec{\tau})\,Y_n^m(\vec{s})=\frac{1}{4\pi}\sum_n^N\sum_{m=-n}^n \bar{I}_n^m(\vec{\tau})\,\bar{Y}_n^m(\vec{s}). \tag{13}$$

The local coefficient functions $\bar{I}_n^m$ are functions of the global I_n^m, and are related by the Wigner-Eckart theorem as [14]

$$\bar{I}_n^m=\sum_{m'=-n}^n D_{mm'}^n I_n^{m'}, \tag{14}$$

where the Wigner $D_{mm'}^n$-functions depend on the three rotation angles from the x-, y- and z-axes.

For the rest of the discussion we will again limit ourselves to two-dimensional geometries in the global x–y-plane, and to the P_3-approximation. For such geometries in local coordinates (with the $\bar{x}$-axis in the x–y-plane) integrals over $\bar{Y}_{2i-1}^m$ vanish for negative m, thus reducing the six boundary conditions to the

required four:

$$\text{for } \bar{Y}_1^0: \bar{I}_0 + \tfrac{2}{3}\bar{I}_1^0 + \tfrac{1}{4}\bar{I}_2^0 = 4\pi I_w, \tag{15a}$$

$$\text{for } \bar{Y}_1^1: \tfrac{2}{3}\bar{I}_1^1 + \tfrac{3}{4}\bar{I}_2^1 = 0, \tag{15b}$$

$$\text{for } \bar{Y}_3^0: \bar{I}_0 - \bar{I}_2^0 - \tfrac{8}{7}\bar{I}_3^0 = 4\pi I_w, \tag{15c}$$

$$\text{for } \bar{Y}_3^1: \tfrac{3}{2}\bar{I}_2^1 - \tfrac{351}{70}\bar{I}_3^1 = 0, \tag{15d}$$

where the boundary intensity I_w has been assumed to be diffuse. Applying the Wigner D-functions this may be expressed in terms of global I_n^m functions as

$$\text{for } \bar{Y}_1^0: I_0 + \tfrac{2}{3}\cos\delta I_1^{-1} - \tfrac{2}{3}\sin\delta I_1^1 - \tfrac{3}{4}\sin 2\delta I_2^{-2} - \tfrac{1}{8}I_2^0 - \tfrac{3}{4}\cos 2\delta I_2^2 = 4\pi I_w, \tag{16a}$$

$$\text{for } \bar{Y}_1^1: \tfrac{2}{3}\sin\delta I_1^{-1} + \tfrac{2}{3}\cos\delta I_1^1 + \tfrac{3}{2}\cos 2\delta I_2^{-2} - \tfrac{3}{2}\sin 2\delta I_2^2 = 0, \tag{16b}$$

$$\text{for } \bar{Y}_3^0: \tfrac{1}{4}I_0 + \tfrac{3}{4}\sin 2\delta I_2^{-2} + \tfrac{1}{8}I_2^0 + \tfrac{3}{4}\cos 2\delta I_2^2 - \tfrac{30}{7}\cos 3\delta I_3^{-3} + \tfrac{3}{7}\cos\delta I_3^{-1} - \tfrac{3}{7}\sin\delta I_3^1 - \tfrac{30}{7}\sin 3\delta I_3^3 = \pi I_w, \tag{16c}$$

$$\text{for } \bar{Y}_3^1: \tfrac{3}{2}\cos 2\delta I_2^{-2} - \tfrac{3}{2}\sin 2\delta I_2^2 - \tfrac{90}{7}\sin 3\delta I_3^{-3} - \tfrac{3}{7}\sin\delta I_3^{-1} - \tfrac{3}{7}\cos\delta I_3^1 - \tfrac{90}{7}\cos 3\delta I_3^3 = 0. \tag{16d}$$

In order to apply these four boundary conditions to the governing Eqs. (11a)–(11d), the I_1^m and I_3^m must be eliminated with the supplementary condition, Eq. (6), by setting $n = 1, 3$, resulting in expressions with derivatives of I_2^0 and I_2^2 in the surface normal direction (local $\bar{z}$-axis) and surface tangential direction (local $\bar{x}$-axis), respectively.

It turns out that, when the surface normal coincides with either the x- or y-axis, boundary conditions $\bar{Y}_1^0$ and $\bar{Y}_3^0$ contain normal derivatives of I_0, I_2^0 and I_2^2, while $\bar{Y}_1^1$ and Y_3^1 contain normal derivatives of only I_2^{-2}. This makes the given set of boundary condition inconvenient for use with commercial PDE solvers, such as FlexPDE [15], which allow "natural boundary conditions" (surface normal derivatives specified). This cannot be achieved by linear combination of the given boundary conditions. Therefore, the $\bar{Y}_3^1$ ($m = 1$) condition is replaced by $\bar{Y}_3^2$ ($m = 2$), which allows, via linear combination, the formulation of four "natural" boundary conditions, i.e.,

$$\frac{\partial I_n^m}{\partial n} = f\left(\frac{\partial I_{n'}^{m'}}{\partial t}, I_{n'}^{m'}\right), \quad n, n' = 0, 2, \; m, m' = 0, \pm 2, \tag{17}$$

which can be used with FlexPDE and other commercial programs.

3. Sample calculations

Several one- and two-dimensional radiative heat transfer problems have been investigated, employing the P_N-approximation developed in this study. First, a check on the consistency of the P_3 governing equations as well as boundary conditions was done by considering a one-dimensional medium being aligned with any of the three primary global coordinates. An absorbing–emitting medium and isotropically scattering medium confined in a rectangular enclosure was studied next, and the results were compared with those obtained from DOM/FVM. Finally, an equilateral triangular enclosure filled with a variable property medium was solved to demonstrate the capability and flexibility of the developed P_N-approximation.

Since the one-dimensional plane-parallel slab has been studied extensively with both analytical and exact numerical solutions available in the literature, it can serve as a quick check for the consistency of the governing equation (8). When an isothermal, absorbing–emitting gray medium is considered, the surface normal can be made to coincide with any of the three global coordinates. If the normal is aligned with the global z-axis, the P_3-approximation reduces to two coupled ODEs in I_0 and I_2^0. However, if the normal points into either the x- or y-direction, three coupled ODEs are obtained instead, consisting of I_0, I_2^0 and I_2^2. It is found that, for all

three different arrangements, the I_2^0 and I_2^2 can be eliminated, leaving the same fourth-order ODE in I_0 independent of the direction of the surface normal. The boundary conditions are also found to be invariant with the choice of coordinate rotation. The solution has been given by Modest [1] with a discussion about the effects of the medium's optical thickness. Consideration of this simple one-dimensional problem demonstrates the validity of the P_3-approximation governing equation (8) and the consistency of the governing equations under rotation of global coordinates.

Sample calculations of two-dimensional heat transfer in a rectangular enclosure have been performed via both the P_3-approximation and the FVM with equivalent order of approximation. The two-dimensional enclosure is placed in the x–y-plane, so that Eqs. (11a)–(11d) are the governing equations. The boundary conditions are provided by Eqs. (16a)–(16c). The radiative transfer results for the P_3-approximation were obtained by using a commercial finite-element PDE solver, FlexPDE [15], while results for the FVM were obtained using a code developed by Chai [16].

The first test problem assumes a square enclosure with side lengths L filled with a gray absorbing–emitting medium at radiative equilibrium. The boundaries are assumed to be cold and black except the bottom one, which is at T_h. Fig. 2 shows a comparison of results with the FVM for the dimensionless local incident radiation ($G^* = I_0/(\sigma T_h^4) = 4T^4/T_h^4$) distribution along the centerline (at $x = L/2$) for different values of optical thickness $\tau = (\kappa + \sigma_s)L$ (note that for a gray medium at radiative equilibrium there is no distinction between absorption–reemission and isotropic scattering [1]). The coupled equations of the P_3-approximation were solved simultaneously on a total of 525 nodes and 242 finite-element cells. Typical computation times on a Pentium 4 2.53 GHz platform were <1 s. The CPU time appeared to be insensitive to the optical thickness.

For comparison, the same problem was also solved using the FVM as shown in Fig. 2. The 4π solid angle in the FVM calculation was divided into 4×4 angles, to make it comparable in order to the total of the 10 spherical harmonics used for the P_3-approximation. For the FVM solution convergence times increased, however, as the optical thickness of the medium increased and CPU time on the same platform doubles to $\simeq 2$ s. In Fig. 2, the "exact" solution was obtained by setting the FVM to the maximum accuracy allowed (24×8 solid angles). From the comparison in Fig. 2 it can be seen that the P_3-approximation consistently outperforms the $FVM_{4\times4}$ method, especially for the optically thin and intermediate cases ($\tau = 0.2, 2$). For optically thick media, both P_3 and the FVM calculations are close to the exact solution, but the FVM requires about twice the CPU time.

In the next sample calculation a rectangular enclosure with four black walls is considered. Only a mid-section ($0.4L < x < 0.6L$) of the bottom wall is hot (T_h), and the rest of the bottom wall and all the other three walls are cold. A homogeneous and purely isotropically scattering medium ($\sigma_s L = 1$; $\kappa = 0$) is confined in the enclosure. The objective is to evaluate the dimensionless heat flux across the right wall for the given medium, in order to compare with DOM results given by Li et al. [17]. Fig. 3 includes results from the P_3-approximation, the LSN S_8 scheme [18], the LSO S_8 scheme [19] and exact Monte Carlo calculations. For LSN S_8 and LSO S_8, the results were obtained by using the step scheme and a 50×50 grid. As shown in Fig. 3, the P_3-approximation yields results comparable in accuracy to the S_8 LSN scheme, which features improvement over the moment-matching DOM scheme such as LSO by reducing ray effects. For this advanced LSN scheme, the weights are determined directly on the basis of geometric and physical considerations, while for the LSO scheme, the weight calculation is done algebraically and, thus, suffers from considerable ray effects [17]. If the DOIM [20] scheme instead of the step scheme was used for the LSN S_8 and

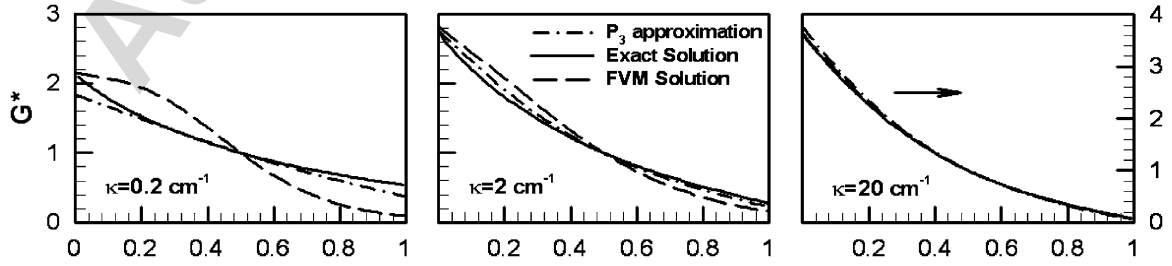

Fig. 2. Dimensionless incident radiation G^* along the centerline at $x = 0.5$.

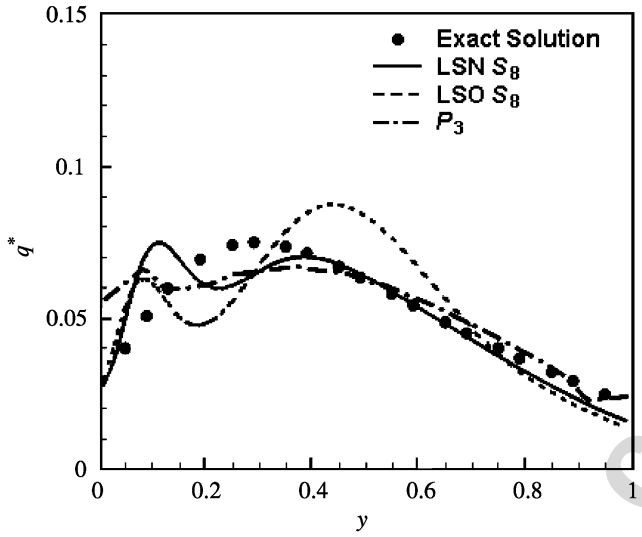

Fig. 3. Comparison of dimensionless heat flux q^* on the right wall.

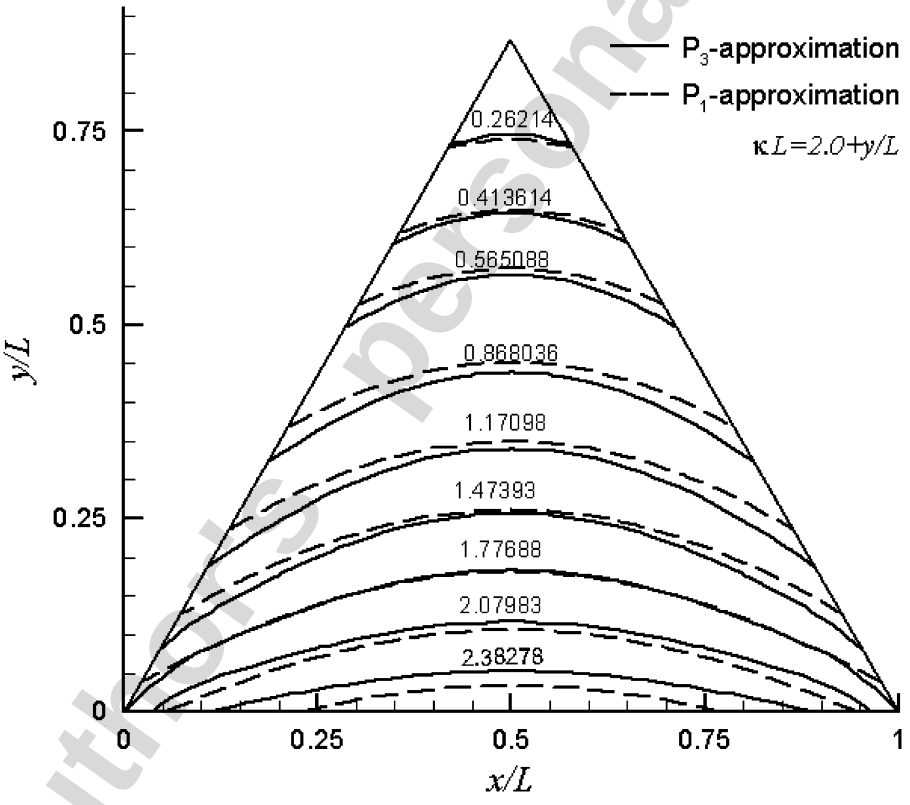

Fig. 4. Comparison of dimensionless G^* with variable medium property in a equilateral triangle enclosure.

LSO S_8, the results [17] become worse due to the ray effect. From this comparison, it is quite apparent that the P_N-approximation is less vulnerable to the ray effect, which is inherent to the DOM.

To demonstrate that the developed P_N-approximation is readily applied to irregular geometries, another sample calculation has been done on a equilateral triangle enclosure with three black walls, where one hot side of the triangle is placed along the x-axis and the other two walls are cold. An absorbing–emitting medium with variable absorption coefficient ($\kappa L = 2.0 + y/L$; L is the side length of triangle) is at radiative equilibrium inside the enclosure. In the absence of an exact solution in the literature for such a complicated case, P_1 results were obtained for comparison with P_3 results. For complex geometries, the P_1-approximation can be easily

implemented, because its governing equation and boundary conditions are in conservative form. As can be seen from Fig. 4, P_1 basically underestimates the dimensionless incident radiation by up to 8% compared to the P_3-approximation near bottom wall locations. However, since the local absorption coefficient increases linearly in the y direction, at the optically thicker top section of the triangle P_3 results show little difference from P_1 results. The computational cost remained below 1 s for this case using FlexPDE [15] on 100 cells with 231 nodes, and CPU time remained unchanged whether a variable property medium is involved or not.

4. Conclusions

A new form of P_N-approximation formulation that can be extended to any order of accuracy has been developed in this study. The resulting governing equation is a set of coupled second-order elliptic PDEs, which can be solved by using commercial PDE solvers. Several two-dimensional radiative heat transfer problems have been studied employing the P_3-approximation based on the proposed method. Comparison was made with available FVM, DOM and exact solutions from Monte Carlo calculations. The following two conclusions can be drawn based on the performance of the P_3-approximation:

(1) Unlike previous developed P_3-approximations, the present method provides a tool to assemble second-order coupled PDEs for any given odd order N, so that any desired order of accuracy can be obtained. These PDEs are compatible with standard PDE solvers. Moreover, the set of the governing equation allows the consideration of variable property media with anisotropic scattering. The generic boundary condition also means that complex geometries can be dealt with without extra work on developing specific boundary conditions. The resulting governing equations have been shown to reduce consistently with the dimensions of the problem considered, and are rotationally invariant.

(2) Comparison with similar order of accuracy DOM or FVM, P_N was found to be superior to DOM/FVM in terms of ray effects and efficiency, especially when scattering and optically thick media are considered. For DOM/FVM, the number of iterations required increased rapidly for more complicated cases while the P_N-approximation remains unaffected by the level of the difficulty. Although the P_N-approximation also suffers from false scattering due to the expansion of intensity into a (smoother) series of spherical harmonics, it outperforms equivalent FVM/DOM schemes.

References

[1] Modest MF. Radiative heat transfer, 2nd ed. New York: Academic Press; 2003.
[2] Chai JC, Lee HS, Patankar SV. Ray effect and false scattering in the discrete ordinates method. Numer Heat Transfer B 1993;24:373–89.
[3] Kofink W. Complete spherical harmonics solution of the Boltzmann equation for neutron transport in homogeneous media with cylindrical geometry. Nucl Sci Eng 1959;6:473–86.
[4] Bayazitoğlu Y, Higenyi J. The higher-order differential equations of radiative transfer: P_3 approximation. AIAA J 1979;17:424–31.
[5] Tong TW, Swathi PS. Radiative heat transfer in emitting–absorbing–scattering spherical media. J Thermoph Heat Transfer 1987;1(2):162–70.
[6] Ratzel AC, Howell JR. Two-dimensional radiation in absorbing–emitting–scattering media using the P–N approximation. ASME J Heat Transfer 1983;105:333–40.
[7] Mengüç MP, Viskanta R. Radiative transfer in three-dimensional rectangular enclosures containing inhomogeneous. Anisotropically scattering media. JQSRT 1985;33(6):533–49.
[8] Davison B. Neutron transport theory. London: Oxford University Press; 1958.
[9] Ou SCS, Liou KN. Generalization of the spherical harmonic method to radiative transfer in multi-dimensional space. JQSRT 1982;28(4):271–88.
[10] MacRobert TM. Spherical harmonics, 3rd ed. New York: Pergamon Press; 1967.
[11] Mark JC. The spherical harmonics method, part I. Technical report, Atomic energy report No. MT 92, National Research Council of Canada; 1944.
[12] Mark JC. The spherical harmonics method, part II. Technical report, Atomic energy report No. MT 97, National Research Council of Canada; 1945.
[13] Marshak RE. Note on the spherical harmonics method as applied to the Milne problem for a sphere. Phys Rev 1947;71:443–6.
[14] Rose ME. Elementary theory of angular momentum. New York: Dover; 1995.
[15] FlexPDE software. Sunol, CA: PDE Solutions Inc.
[16] Chai JC, Lee HS, Patankar SV. Finite volume method for radiation heat transfer. J Thermoph Heat Transfer 1994;8(3):419–25.

[17] Li HS, Flamant G, Lu JD. Mitigation of ray effects in the discrete ordinates method. Numer Heat Transfer B 2003;43(5):445–66.
[18] El Wakil N, Sacadura J-F. Some improvements of the discrete ordinates method for the solution of the radiative transport equation in multidimensional anisotropically scattering media. In: Developments in radiative heat transfer HTD-203. New York: ASME; 1992. p. 119–27.
[19] Fiveland WA. The selection of discrete ordinate quadrature sets for anisotropic scattering. In: Fundamentals of radiation heat transfer HTD-160. New York: ASME; 1991. p. 89–96.
[20] Cheong KB, Song TH. An alternative discrete ordinates method with interpolation and source differencing for two-dimensional radiative transfer problems. Numer Heat Transfer B 1997;32:107–25.